Journal of Power Sources 557 (2023) 232570

Contents lists available at ScienceDirect

Journal of Power Sources

journal homepage: www.elsevier.com/locate/jpowsour

Synergistic role of functional electrolyte additives containing phospholane-based derivative to address interphasial chemistry and phenomena in NMC811||Si-graphite cells

Bahareh A. Sadeghi [a], Christian Wölke [a], Felix Pfeiffer [a], Masoud Baghernejad [a], Martin Winter [a,b], Isidora Cekic-Laskovic [a,*]

[a] Helmholtz-Institute Münster, IEK-12, Forschungszentrum Jülich GmbH, Corrensstraße 46, 48149, Münster, Germany
[b] University of Münster, MEET Battery Research Center, Corrensstrasse 46, 48149, Münster, Germany

HIGHLIGHTS

- Novel phospholane additive enhances performance of the NMC811||SiC cell chemistry.
- Decomposition of phospholane additive on cathode and adsorption on anode.
- Synergistic impact of VC and phospholane-based additives.
- Significantly improved cell performance compared to FEC counterpart.

GRAPHICAL ABSTRACT

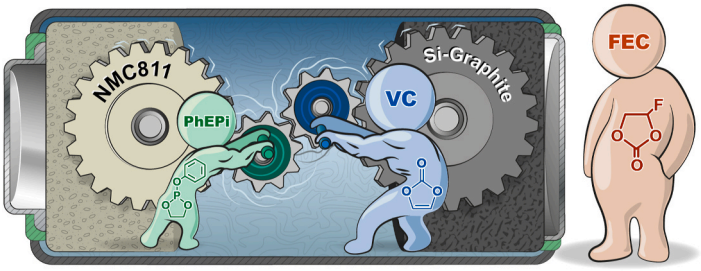

ARTICLE INFO

Keywords:
Non-aqueous aprotic electrolyte
Electrode|electrolyte interface
Synergistic effects
Functional additive
Phospholane-based molecules

ABSTRACT

Herein, we report on the 2-phenoxy-1,3,2-dioxaphospholane (PhEPi) molecule as a novel functional phospholane-based electrolyte additive. The presence of PhEPi in optimal concentration in the baseline electrolyte (EC:EMC 3:7, 1 M $LiPF_6$) significantly enhances the electrochemical performance of the NMC811||Si-graphite cell chemistry. To further optimize the cell's overall performance, two well-known film-forming additives, namely, vinylene carbonate (VC) and fluoroethylene carbonate (FEC), were used as co-additives with PhEPi, and the resulting cells thoroughly characterized by selected electrochemical and spectroscopic techniques. The addition of PhEPi to the VC-containing electrolytes showed the complementary advantages of high specific discharge capacity and prolonged cycle life of the considered cells and outperformed the overall performance of the FEC counterpart. To gain better understanding of the role of each additive on the individual positive and negative electrode interphases, we conducted a systematic investigation of both electrodes, which were pre-cycled against Li-metal electrode. *Post mortem* spectroscopic investigations of the corresponding interphases provided insights into the synergistic effect of VC and PhEPi in the NMC811||Si-graphite cell chemistry.

* Corresponding author.
E-mail address: i.cekic-laskovic@fz-juelich.de (I. Cekic-Laskovic).

https://doi.org/10.1016/j.jpowsour.2022.232570
Received 29 September 2022; Received in revised form 16 December 2022; Accepted 20 December 2022
Available online 29 December 2022

1. Introduction

Lithium-ion batteries (LIBs) are one of the most effective energy storage systems [1,2]. Intensive research has been devoted to the transition from conventional to next-generation LIBs by developing alternative positive and negative electrode materials with higher theoretical specific capacities. For this reason, Si-based negative electrodes [3,4] and nickel-rich positive electrodes [5] were recognized as two viable examples of LIBs' next-generation electrode materials. However, due to their interfacial/interphasial instabilities, batteries containing the aforementioned active materials often experience rapid failure [6]. This failure results from irreversible phase transitions, transition metal dissolution, and oxygen evolution during charge/discharge cycling on the positive electrode side (*e.g.* $LiNi_xMn_yCo_zO_2$, NMC_{XYZ}) [7]. On the other side, a significant volume expansion of Si-based negative electrodes during (de-)lithiation leads to surface structure cracking and renewed interphase formation in each cycle [8–10]. It should be noted here that in addition to different solid electrolyte interphase (SEI) dynamics of intermetallic (*e.g.* Si.) and carbonaceous anode materials (*e.g.* graphite) [11,12], there are also notable differences in regard to electrolyte decomposition and SEI formation mechanisms [13]. Tailoring the electrolyte composition and the resulting formulation to tackle the failure mechanism imposed by Si- and NMC-based electrodes represents one of the major challenges. It is believed that many of the aforementioned failure modes in NMC and Si-based electrodes can be overcome by the formation and controllable dynamics of a flexible, but still robust interphase. It is consequently critical to developing high-performance electrolyte formulations to modify the interphase characteristics, enabled by replacing or adding the right combination of functional electrolyte components *i.e.* conducting salt, solvent/co-solvent, or functional/multifunctional additives in an optimum amount [14]. Incorporating functional electrolyte additives into baseline electrolyte formulations is shown to be one of the most effective and cost-favorable strategies. Functional additives can be sacrificially reduced and/or oxidized at corresponding electrodes to form effective protective layers on the negative and the positive electrode, known as SEI [15] and cathode-electrolyte interphase (CEI [16]), respectively [8,17]. The presence of an effective interphase(s) can suppress the parasitic reactions on the electrodes resulting in a lower irreversible active Li loss [18] rate during cell performance [19]. The importance of interphases to suppress parasitic reactions of charged electrodes with the electrolyte has been first addressed in a comprehensive SEI model by Peled and co-workers [15].

Up to now, there are a number of electrolyte additives that have shown a significant influence on LIB cell performance. Fluoroethylene carbonate (FEC) is the most investigated electrolyte co-solvent/additive for Si-based anodes, followed by vinylene carbonate (VC) [8]. Despite beneficial effects [20,21], due to the presence of fluorine, FEC is a rather cost-intensive additive, which may significantly impact the overall cost of the resulting electrolyte. This effect is particularly evident when FEC is implemented into the electrolyte formulation at the common ten weight/volume percent [22]. Additionally, FEC contains fluorine, which is considered as environmentally unfriendly and raises ecological concerns [10,23–25]. There are possibilities as solutions to this challenge, either to combine FEC with co-additives with complementary functionalities or to replace it with an alternative additive that has similar beneficial implications at the anode [26].

As mentioned, VC is widely recognized as a film-forming additive that stabilizes the SEI, which is predominantly generated during the first cycle prior to the decomposition potentials of the electrolyte solvent molecules, such as ethylene carbonate (EC) and linear carbonates like ethyl methyl carbonate (EMC) and dimethyl carbonate (DMC) [27–29]. As a result, presence of VC additive enhances galvanostatic cycling performance and decreases irreversible capacity loss of the cell. Rayan and co-workers showed that 3 wt% VC as an electrolyte additive on the Si-nanowire electrode outperforms FEC [30]; even at 60 °C, it was identified as the most effective additive for this particular anode [23]. One of the reasons for observing this improvement is due to the formation of a dense poly(VC) film on the negative electrode surface, prohibiting the solvent molecules from reaching the active Si and thus diminishing innevitable parasitic reactions [17,31]. On the other hand, they found that VC containing electrolytes suppress the initial discharge capacity of the overall cell, related to the low Li-ion conductivity of the formed poly(VC) film on the surface [23]. VC can be considered a feasible alternative to FEC as this molecule contains no fluorine in the structure, has a lower cost [32], and according to the literature, has a comparable influence to FEC on performance of the Si-based anode cells [8,17,23]. Our previous studies showed that phospholane-based additives have the potential to stabilize the electrode|electrolyte interface by forming an effective CEI on the positive electrode, thus enhancing the overall cell performance [33]. Due to its characteristics, such as film-forming ability and flame-retardancy, class of phospholane-based additives is a suitable candidate for high-voltage applications and enhanced safety performance [34]. The film-forming ability of the phospholane-based additives results from the ring-opening reaction on the positive electrode and subsequent polymerization, which prevents further electrolyte decomposition [2,23,24]. Among several novel derivatives, the 2-phenoxy-1,3,2-dioxaphospholane (PhEPi) additive showed the most promising characteristics. Within this work we introduce PhEPi into the baseline electrolyte (BE; 1 M $LiPF_6$ in EC:EMC 3:7 by vol.), compared to reference electrolyte (1 M $LiPF_6$ in EC:EMC 3:7 by vol. + 10% FEC) to enhance the galvanostatic cycling performance while reducing/eliminating the FEC content. A practical approach that is utilized in this work comprises simultaneous implementation and investigation of PhEPi with FEC and/or VC to enhance the galvanostatic cycling performance of the resulting cell chemistry. The significant influence of phospholane-based additives on CEI can be combined in a synergistic approach with SEI additives to bring additional enhancement to the overall cell performance. The synergistic effect of the co-additives with PhEPi was studied by selected complementary electrochemical and spectroscopic techniques. A systematic investigation of positive and negative electrodes that were pre-cycled *vs*. Li-metal was conducted to understand the role of each additive on the individual electrode interphases.

2. Experimental section

2.1. Materials and synthesis

2.1.1. Synthesis of the phospholane-based derivative and characterization

Ethylene chlorophosphite (97%) was purchased from Alfa-Aesar. Phenol (99.5%) was purchased from Sigma-Aldrich. Pyridine (99%) was purchased from TCI. Diethylether (99%), Celite 545 and 3 Å molecular sieves beads were purchased from Merck. Et_2O was dried using a PureSolv solvent purification system (Inert Corporation), pyridine was dried over Na and distilled, and stored over 3 Å molecular sieves under Ar before use. PhEPi was synthesized in flame-dried glassware under an argon atmosphere using standard Schlenk-techniques following a modified literature procedure [35]. 2-Chloro-1,3,2-dioxaphospholane (6.0 mL, 67.5 mmol) and pyridine (5.4 mL, 67.5 mmol) were dissolved in dry Et_2O (200 mL), and the solution was cooled to 0 °C. Thereafter, a solution of phenol (6.36 g, 67.5 mmol) in dry Et_2O (50 mL) was added dropwise over a period of 5 min, leading to the formation of a white precipitate. The suspension was allowed to warm to room temperature and was stirred for 24 h. After filtering through a plug of Celite, the solvent was removed with a condensation trap at room temperature under a pressure of 40 mbar. Fractioned distillation of the residue through a Vigreux column yielded the product (6.547 g, 52%; 47 °C, 0.4 mbar) as a colorless liquid (Scheme 1).

^{1}H NMR (400 MHz, 300 K, Benzene-d_6): $\delta = 7.05$ (m, 2H, *o*-Ph), 6.99 (m, 2H, *m*-Ph), 6.82 (m, 1H, *p*-Ph), 3.60 (m, 2H, CH_2), 3.29 (m, 2H, OCH_2).

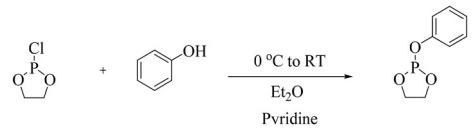

Scheme 1. Synthesis route of PhEPi.

$^{13}C\{^1H\}$ NMR (101 MHz, 300 K, Benzene-d_6): δ = 152.48 (d, $^2J_{CP}$ = 3.4 Hz, *i*-Ph), 129.95 (*m*-Ph), 124.01(d, $^5J_{CP}$ = 1.1 Hz, *p*-Ph), 121.08 (d, $^4J_{CP}$ = 6.9 Hz, *o*-Ph), 64.10 (d, $^2J_{CP}$ = 8.8 Hz, CH_2).

$^{31}P\{^1H\}$ NMR (162 MHz, 300 K, Benzene-d_6): δ = 128.8.

2.1.2. Electrolyte components and electrode materials

NMC811 single-sided electrode sheets with 1.67 mAh•cm^{-2} and Si-graphite single-sided electrode sheets with 2 mAh•cm^{-2}, containing 20% silicon, purchased from Targray, were kept in the dry room (dew point < −60 °C) and dried for 12 h at 120 °C under vacuum (10^{-2}-10^{-3} mbar) prior to use. Thereafter, they were stored in the argon-filled glovebox (MBraun Labmaster, H_2O and O_2 content <0,5 ppm). Li metal (500 μm thickness) purchased from China Energy Lithium CO. Ltd was kept inside the argon-filled glovebox as well. Celgard 2500 as a separator for 2032-type coin cells and Whatman grade GF/D (10, 13 mm) as a separator for Swagelok T-cells were dried overnight at 60 °C and stored in the argon-filled glovebox. All considered electrolyte solvents (EC, EMC, FEC) and conducting salt ($LiPF_6$) were provided by Solvionic Co. in battery grade, including the baseline electrolyte (1 M $LiPF_6$ in EC:EMC 3:7 by vol.). VC was purchased from E–Lyte Innovations. The resulting electrolyte formulations were stored in the argon-filled glovebox.

2.2. Electrolyte formulation and cell assembly

1 M $LiPF_6$ in EC:EMC (3:7 by vol.) was used as a baseline electrolyte (BE). All considered electrolytes were formulated by adding different concentrations of PhEPi and $LiPF_6$ by molar ratio and different amounts of FEC/VC by weight percentage to an EC:EMC (3:7 by vol.) stock solution in a volumetric flask. All considered cells were assembled in an argon-filled glovebox (MBraun Labmaster, H_2O and O_2 content <0,5 ppm). For all galvanostatic cycling measurements, two-electrode [36] 2032-type coin cells with one layer of Celgard 2500 separator and 35 μL of electrolyte were assembled. For assembling cells with pre-cycled electrodes (section 3.3.1), the electrodes were first cycled *vs.* Li metal electrodes using different electrolytes for the three formation cycles. The cells were thereafter disassembled and reassembled in a two-electrode NMC811||SiC configuration after rinsing the pre-cycled electrodes with 1 mL EMC. Then galvanostatic cycling was continued with the reassembled cells.

For cyclic voltammetry measurements (CV), 3-electrode Swagelok T-cells with one layer of Whatman grade GF/D (10, 13 mm) as the separator and 200 μL of electrolyte were assembled with SiC or NMC811 electrodes as a working electrode and Li metal as counter and reference electrodes.

2.3. Electrochemical characterization

CV measurements were conducted using a VSP potentiostat (Bio-Logic) at a scan rate of 0.025 mV s^{-1} in a 3-electrode setup. The cells were cycled for three cycles in the potential range from 3.4 to 5 V *vs.* Li|Li$^+$ for NMC811 or from 0.01 to 1.5 V *vs.* Li|Li$^+$ for SiC, starting from the open circuit potential (OCP).

Galvanostatic cycling measurements were performed on a battery tester (MACCOR series 4000 and Arbin BT-2X43) in the voltage range of 2.8 V–4.2 V. After 6 h rest, three formation cycles of the cells were conducted at C/10. After formation, the cells were galvanostatically cycled at C/3 for 100 cycles.

For SiC||Li cells, the theoretical capacity was multiplied by 0.835 to account for the electrode's N/P ratio and mimic the current density of NMC811||SiC cells. After formation, NMC811||Li and SiC||Li cells were dissembled, reassembled in NMC811||SiC configuration and cycled at C/3 for 100 cycles.

2.4. Electrochemical impedance spectroscopy

Electrochemical impedance spectroscopy (EIS) measurements were carried out at a Bio-Logic VMP3 workstation. First, two-electrode cells were galvanostatically cycled for formation, then based on the work of Petibon et al. [37] charged to 50% state-of-charge (SOC). Full cell impedance was measured at a range of 10 mHz–100 KHz after 30 min of rest time. Thereafter, the coin cells were disassembled, and symmetric cells with 35 μL of the same electrolyte were reassembled and impedance spectra of the symmetric cells recorded.

2.5. X-ray photoelectron spectroscopy

XPS measurements were carried out at a 0° angle of emission and a pass energy of 200 eV using a monochromatic Al Kα source (Ephoton = 1486.6 eV) with a 10 mA filament current and a filament voltage source of 12 kV. The analyzed area had approximately 400 μm spot size. A charge neutralizer was used in order to compensate for the charging of the sample. The F 1s peak at 684.8 eV (LiF) was taken as an internal reference for the adjustment of the energy scale in the spectra. To avoid any contact with oxygen and/or moisture, considered XPS samples were sealed in vials for transfer to the measurement device after preparation. The sealed vials were stored and opened in a mini glovebox connected to the XPS device shortly before measurement. CasaXPS software was used for fitting the measured spectra and Peaks assigned in accordance with known literature values [38,39].

2.6. Raman spectroscopy

For Raman investigation of the interphases, a Horiba Scientific confocal Raman microscope (LabRAM HR evolution, air-cooled CCD detector) was used. Sample excitation was conducted by a red laser (wavelength of 633 nm) and an output power of 10.5 mW at the sample, which was adjusted by a 10% filter to 1.05 mW with a 600 line/mm grating. The laser was focused using a 50X long-working distance objective (Zeiss, 9.2 mm, numerical aperture 0.5). Raman spectra were collected using three 35-second integrations. LabSpec6.6.2 was used to operate the Raman microscope, collect spectra, and analyze the data (Horiba Scientific). Before the measurement, the system was calibrated on the silicon band at a Raman shift of 520.7 cm^{-1}.

2.6.1. Shell-isolated nanoparticle-enhanced Raman spectroscopy (SHINERS) sample preparation

The utilized Au-nanoparticles (NPs) were synthesized by citrate reduction of an Au(III)-solution, following the procedure of Li et al. [40] For the investigation, NPs with the size of 55 nm were synthesized. Before application, the NPs were coated with a silica shell using a hydrolyzed sodium silicate solution. The shell had a thickness of approximately 4 nm. For applying the coated NPs to the surface of the investigated electrode, the silica-coated nanoparticles were transferred into isopropanol, subsequently drop-casted on an optical window, and dried in the oven before transferring to the argon-filled glovebox. The optical window was brought in contact with the surface of the electrodes on the NP-coated side for the SHINERS measurements. An airtight optical cell (EL-CELL ECC-Opto-Std) was used for all Raman measurements. The considered electrodes were harvested from NMC811||SiC coin cells, which were cycled for three formation cycles at the rate of 0.1 C between 2.8 and 4.2 V. After formation, the cells were charged to 50% SOC and opened in an argon-filled glovebox to extract the electrodes for SHINERS investigation.

3. Results and discussion

3.1. Electrochemical characterization

To determine the electrochemical stability of the PhEPi containing electrolyte formulations, cyclic voltammetry measurements were performed. The oxidative stability of PhEPi on NMC811 is represented in Fig. 1a and **b**. Decomposition of PhEPi is observed in the first cycle (Fig. 1a) by the broad peak starting at 4.3 V *vs.* Li|Li$^+$. The subsequent cycles in Fig. 1b reveal the absence of this peak, indicating PhEPi decomposition taking place only in the first cycle. As shown in Fig. 1c, no cathodic decomposition peak of PhEPi could be observed. Fig. 1d displays the cyclic voltammogram of the PhEPi containing electrolytes with/without VC as co-additive. By comparing these two graphs, a peak around 4.9 V *vs.* Li|Li$^+$ can be attributed to VC decomposition.

3.2. Impact of PhEPi additive on galvanostatic cycling performance

Galvanostatic cycling of NMC811||SiC cells was performed to evaluate the performance of PhEPi and of the co-additives, both as single additive and in a mixture with VC. In order to identify the optimum amount of considered additives, a concentration screening in the range of 0–2 M for PhEPi and 0 to 10 wt% for the co-additives was performed (Fig. S1). Fig. 2a shows the cycling performance of cells with electrolytes containing the respective optimum amounts of single PhEPi and VC additives, as well as the combination thereof. The presence of PhEPi in the optimum amount in NMC811||SiC cells significantly improves the initial specific discharge capacity compared to the BE containing counterpart, as depicted in Fig. 2a. The first cycle specific discharge capacity of PhEPi containing cells starts at 183 mAh•g^{-1}, whereas the value for the BE-containing counterpart amounts to 160 mAh•g^{-1}. Furthermore, the first cycle specific discharge capacity of the cells containing 10% FEC and 8%VC has a lower value compared to the cells containing PhEPi as well (157 and 153 mAh•g^{-1} for FEC and VC, respectively). For a deeper observation of the fading rate, the capacity retention (CR) was normalized by the fourth cycle. The CR of cells containing no additive reaches 80% after the 16th cycle. Despite the increased discharge capacity, the addition of PhEPi to the electrolyte has no significant impact on the CR. Although the specific discharge capacity in the first cycles is lower for VC containing cells compared to the baseline electrolyte containing counterpart, capacity fading is much less pronounced. For FEC containing cells, no drop in initial discharge capacity was observed. However, the improvement of capacity fading is significantly less pronounced than for the VC containing counterparts. As a consequence, the FEC containing cells reach 80% state of health (SOH) after 20 cycles compared to 25 cycles for the VC containing counterparts.

In line with this, we combined PhEPi with FEC or VC to further enhance the galvanostatic cycling performance. Surprisingly, we observed that the combination of PhEPi with VC has a superior impact on the overall cell performance regarding higher initial specific discharge capacity than for VC alone, less fading, higher coulombic

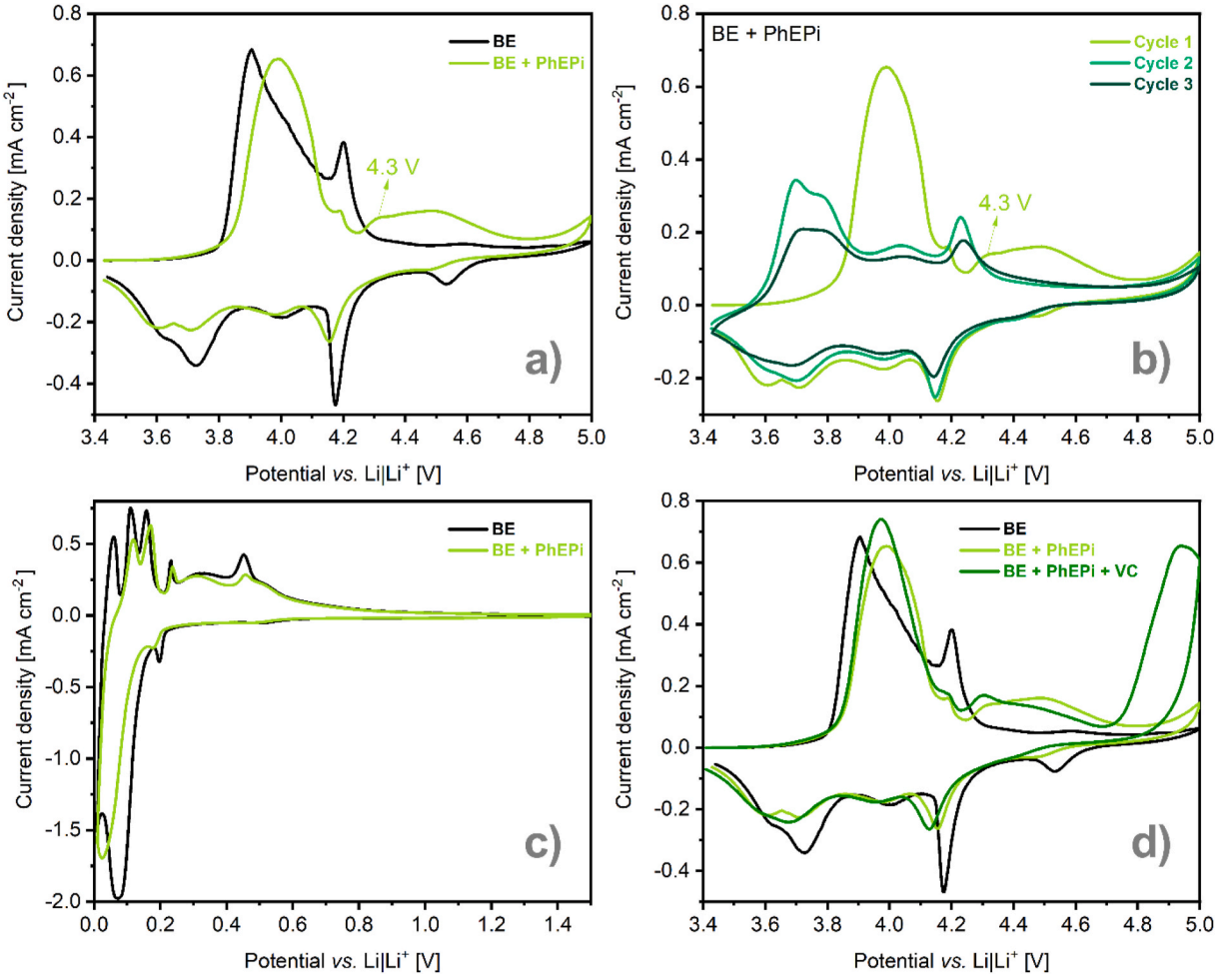

Fig. 1. (a) First cycle cyclic voltammograms on NMC811 for 1 M $LiPF_6$ in EC:EMC 3:7 by vol. (BE) and BE + 0.038 M PhEPi (BE + PhEPi) (b) Cyclic voltammograms of consecutive cycles on NMC811 with PhEPi containing electrolyte (c) First cycle cyclic voltammograms on SiC for electrolyte formulations BE and BE + PhEPi (d) Comparison of the first cycle cyclic voltammograms on NMC811 for BE + PhEPi and BE + PhEPi + VC.

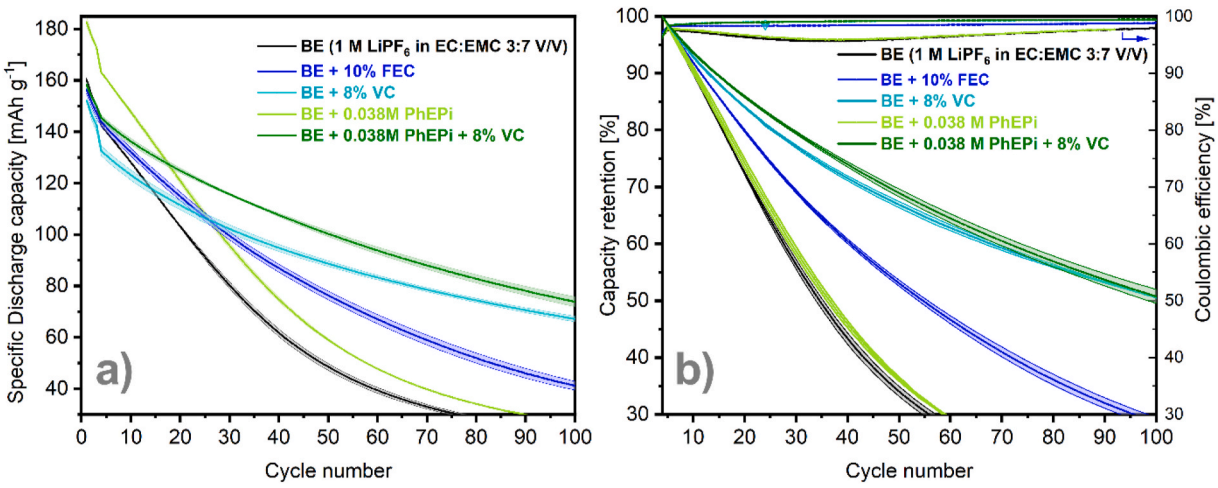

Fig. 2. (a) Specific discharge capacity of NMC811||SiC cells with considered electrolytes (b) Coulombic efficiencies and capacity retentions of NMC811||SiC cells with different electrolytes.

efficiency, and prolonged cycle life, while no improvement was observed for the cells containing the combination of FEC and PhEPi (Fig. S2). A similar performance trend was observed by comparing the performance of FEC/PhEPi electrolyte formulations to FEC containing counterparts, indicating that FEC shows poorer compatibility and an absence of synergestic effects with PhEPi. The obtained results

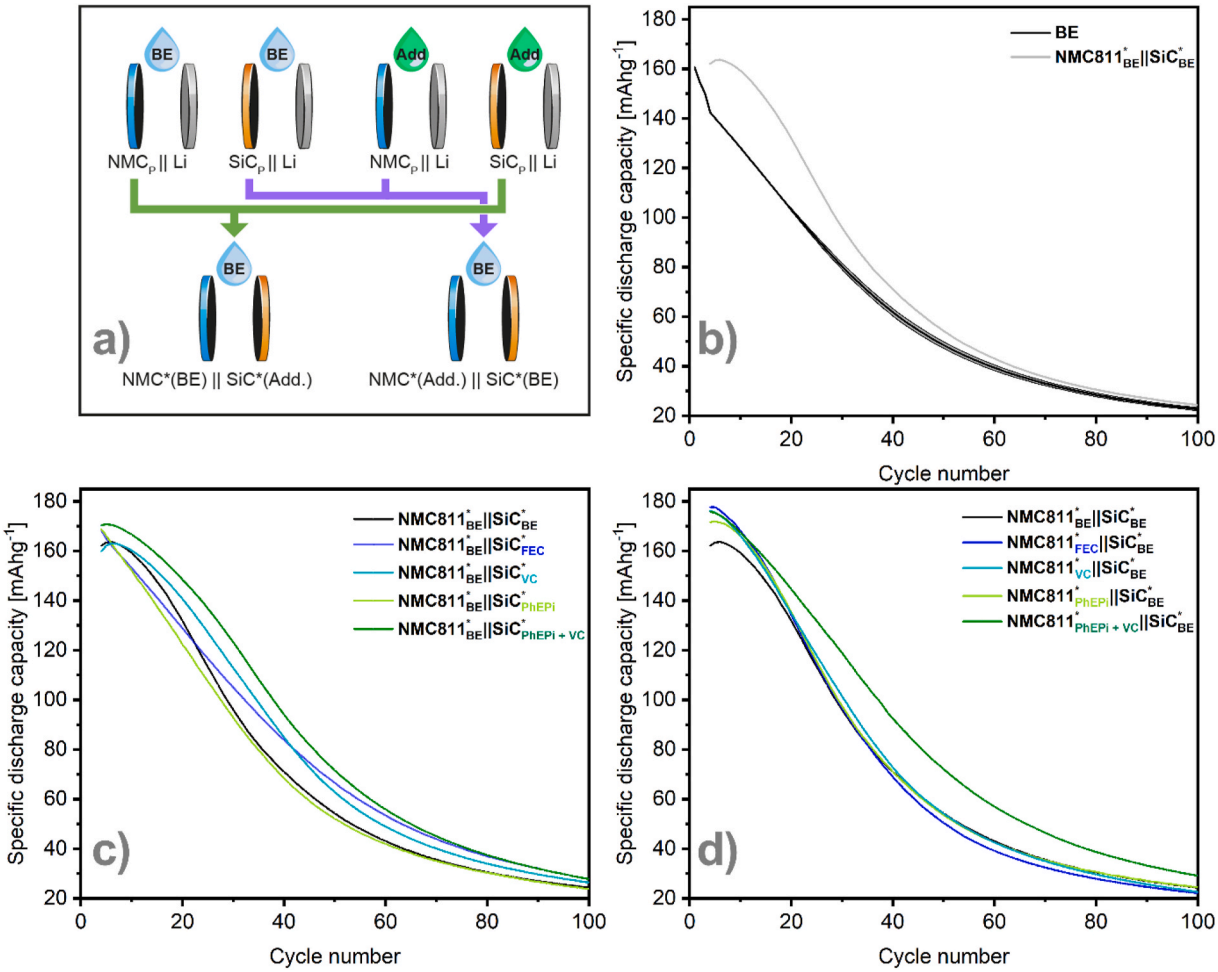

Fig. 3. (a) Schematic diagram illustrating the systematic cell disassembly-reassembly strategy for investigation of the direct impact of pre-formed SEI and CEI in the presence of functional additives on full cell performance. (b) Galvanostatic cycling performance of reassembled cells compared to regular cells using only BE. (c) Galvanostatic cycling performance of reassembled cells with pre-cycled NMC811 with the considered additive-containing electrolytes against SiC pre-cycled with the BE. (d) Galvanostatic cycling performance of reassembled cells with SiC pre-cycled in the considered additive-containing electrolytes against NMC811 pre-cycled in the BE.

demonstrate that a combination of PhEPi and VC at an optimum amount is indeed able to synergistically combine the improved CR of VC with the increased discharge capacity caused by PhEPi. The important role of synergistic effects in such electrolyte formulations is reviewed in literature [14].

3.3. Synergistic role of additives on the interphases(s)

3.3.1. Galvanostatic characterization through cell disassemble-reassemble strategy

To understand the impact of PhEPi with and without co-additives on the individual electrodes during SEI and CEI formation, we applied a systematic cell disassembly-reassembly strategy. Similar strategies have been reported by other groups previously [41–43]. The process is schematically represented in Fig. 3a. First, we galvanostatically cycled cells containing either NMC811 or SiC as working electrode and Li metal the counter electrode for three formation cycles with the considered electrolyte formulations (BE, BE + 0.038 M PhEPi, BE + 8% VC, BE + 10% FEC, BE + 0.038 M PhEPi + 8%VC). In the next step, we disassembled the cells, washed the electrodes with EMC, and reassembled the individual pre-cycled electrodes against the counterpart pre-cycled electrodes using the baseline electrolyte. One reason for using the counterpart pre-cycled electrode instead of pristine electrodes in the reassembled cell relates to different SOC of pristine and "fully discharged" electrodes; even when at lower cut-off voltage, the electrodes are not fully (de-)lithiated, which has to be taken into consideration whenever galvanostatically pre-cycled electrodes are combined with not-cycled ones. In order to make a reasonable comparison, both electrodes must be in a similar SOC . We therefore applied a 0.835 factor to the capacity of SiC electrodes in SiC||Li cells to account for the N/P ratio and mimic the current density the electrode would be subjected to in a typical NMC811||SiC cell. The results of the reassembled cells containing pre-cycled electrodes with pristine electrodes are available in the supporting information (Fig. S3).

As a common process, the extracted electrodes were washed with EMC or DMC to wipe out residuals of conducting salt ($LiPF_6$) and then dried to remove volatile organic solvents [44–47]. Due to the unknown effect of washing steps on the electrochemical performance of the electrodes and interphase properties [44,45,48], we considered minimizing the washing time to 30 s with 1 mL of EMC for washing the pre-cycled electrodes, instead of considerably longer washing time reported previously [27–29]. To account for any performance impacts due to the disassembly-reassembly process and make a fair comparison, we applied it to a batch of cells with baseline electrolyte only. As can be seen in Fig. 3b, cells that underwent the disassembly-reassembly protocol with baseline electrolyte show a significantly increased discharge capacity compared to regular cells cycled with the baseline electrolyte, as well as a pronounced curvature of the capacity profile. Since in the pre-cycling, the electrodes are paired with Li metal, *i. e.* an unlimited source of lithium, any losses of lithium inventory through interphase formation can be compensated. If aforementioned electrodes are then used for reassembly, the cells have an artificially increased lithium inventory, thus resulting in an increased discharge capacity. Therefore, these reassembled cells (NMC^*_{BE}||SiC^*_{BE}) were used as the reference for the comparison of results.

Fig. 3c compares the specific discharge capacity profiles of cells with SiC electrodes that were pre-cycled in considered additive-containing electrolytes and NMC811 electrodes that were pre-cycled with the BE. An asterisk indicates a pre-cycled electrode followed by the electrolyte used in pre-cycling. All cells were reassembled with the BE. In these series of cells, we considered NMC^*_{BE}||SiC^*_{BE} as the benchmark system. As can be seen in this graph, the use of SiC^*_{PhEPi} leads to only a slight increase in specific discharge capacity as opposed to the regular cell, while no improvement of capacity fading can be observed. In the case of SiC^*_{FEC}, a similar specific discharge capacity but a lower rate of fading was observed. The use of SiC^*_{VC} does not impact the specific discharge capacity compared to the baseline but leads to an initially lower fading rate compared to SiC^*_{FEC}, which increases as galvanostatic cycling progresses and eventually overtakes the fading rate with SiC^*_{FEC}. When $SiC^*_{PhEPi+VC}$ is used, just as in regular cells, a combination of the benefits of both functional additives can be observed. These cells achieve a higher specific discharge capacity than the cells using SiC^*_{PhEPi} and show a similar fading rate to the cells using SiC^*_{VC}. From these results, it can be concluded that in the functional additive combination of PhEPi and VC, the latter component has the major impact on the formed SEI, accompanied by the positive effect originating from the presence of PhEPi. Fig. 3d compares the specific discharge capacity profiles of cells with NMC811 electrodes that were pre-cycled in different additive-containing electrolytes and SiC pre-cycled in the BE. In this case, the use of electrodes pre-cycled with an electrolyte containing any single additive (considered in this study) leads to an increase in the initial specific discharge capacity. As opposed to the SiC side, $NMC811^*_{PhEPi}$ leads to the lowest improvement. The fading is, however, very similar in all cases and quickly leads to a similar specific discharge capacity profile as the baseline. Interestingly, while cells using $NMC811^*_{PhEPi+VC}$ show a similar initial specific discharge capacity, the fading is much less pronounced than for either $NMC811^*_{PhEPi}$ or $NMC811^*_{VC}$, leading to a significantly improved overall performance. The distinct difference of $NMC811^*_{PhEPi+VC}$ to the other individual additives clearly shows that both PhEPi and VC act synergistically on the positive electrode.

In summary, the employed disassembly-reassembly strategy gave clear indications that PhEPi and VC act synergistically and impact both the SEI and CEI with the more pronounced synergy on the positive electrode.

3.3.2. EIS investigations

The influence of PhEPi containing electrolyte formulation on the positive and negative electrode impedance was investigated by means of electrochemical impedance spectroscopy (EIS). Nyquist plots for symmetric NMC811 and SiC cells are shown in Fig. 4a and **b**. It can be observed that the addition of VC to the BE does not significantly impact the CEI resistance, but it strongly affects the SEI resistance, which was reported to be caused by the formation of a poly(VC) layer as a result of VC polymerization [23,49,50]. It can be seen that the addition of PhEPi to VC containing electrolytes affects the internal cell resistance. By looking at the second semi-circle, which represents the impedance of CEI [51,52], significant growth in the presence of PhEPi compared to the BE or VC alone is observed, thus indicating PhEPi decomposition on the cathode during the formation cycles. By comparing these two plots, we can conclude that on the NMC811 side, PhEPi plays a dominant role, but on the SiC side, VC contributes significantly to the resistance of the SEI. These observations are in good agreement with previous work pointing to the fact that phospholane additives likely decompose on the positive electrode and are thus involved in CEI formation [10].

3.4. Post mortem spectroscopic characterization of interphases

3.4.1. Cathode electrolyte interphase characteristics on NMC811

In order to gain a better understanding of the additives' role in the SEI and CEI composition, *post mortem* Raman and XPS analysis was performed on the NMC811 and SiC electrodes after three formation cycles in the NMC811||SiC cell configuration. Raman band assignment on SiC and NMC811 was performed for some of the considered electrolyte formulations (BE, BE + 0.038 M PhEPi, and BE + 0.038 M PhEPi + 8% VC), as depicted in Fig. 5a and **b**. Additionally, the elemental composition of the SEI and CEI surfaces as determined by integration of the XPS spectra for the considered electrolytes are provided in Fig. 6. In Raman spectra, for the NMC electrode in the presence of BE, mostly the peaks for the NMC active materials and the graphitic materials as the conductive phase were observed. In addition, minor bands around 1245, 1465, and 1521 cm^{-1} were observed, which can be assigned to C–H and C═O stretching vibrations of organic compounds of the CEI (*e.g.*,

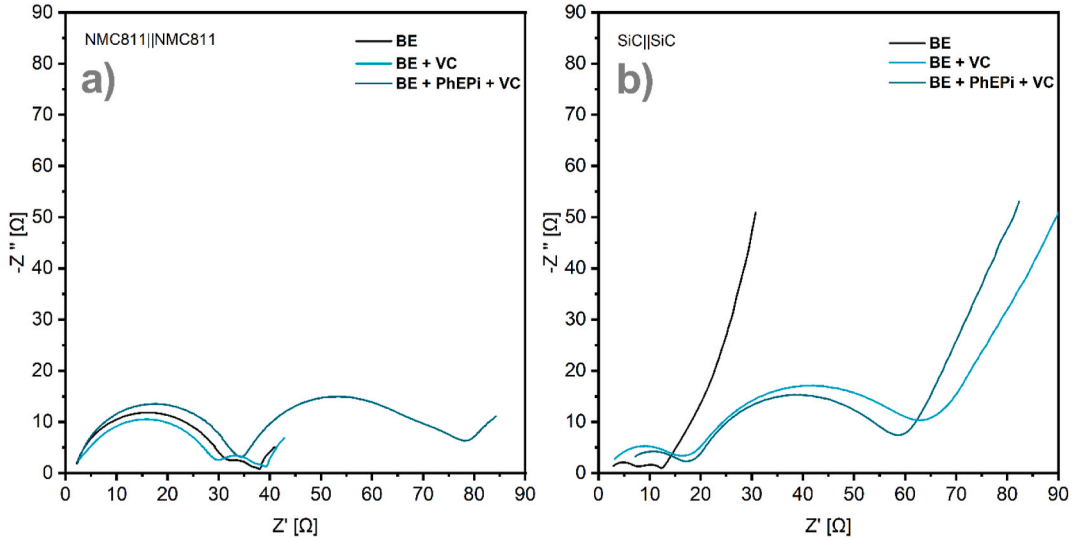

Fig. 4. (a) Nyquist plot of symmetric NMC811 cells assembled from galvanostatically cycled NMC811||SiC cells containing considered electrolytes. (b) Nyquist plot of symmetric SiC cells assembled from galvanostatically cycled NMC811||SiC cells containing considered electrolytes.

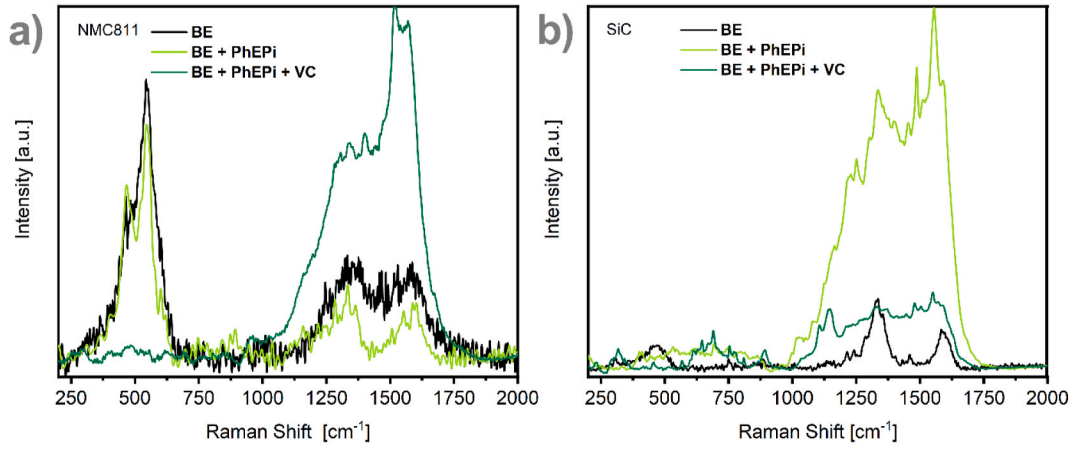

Fig. 5. (a) Raman spectra of the NMC811 electrodes from cells cycled with considered electrolytes. (b) Raman spectra of the SiC electrodes from cells cycled with considered electrolytes.

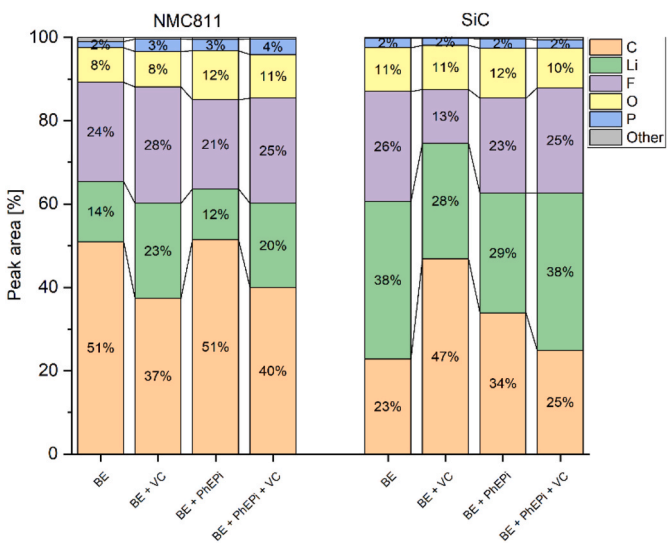

Fig. 6. The elemental composition of interphase layers on NMC811 and SiC probed by XPS for the considered electrolyte formulations.

$ROCO_2Li$) derived from electrolyte decomposition [53–55]. Nevertheless, these bands have very low intensities, showing a very low amount of these compounds on the cathode surface. For considered electrodes, regardless of the electrolyte composition, the C 1s spectra (Fig. 7a) comprised several distinct peaks assigned to the following bond types: C–C/C–H (~284.0 eV), C–O (~286.0 eV), C═O/O–C–O/O═C–O (287–289 eV) and CO_3 species (~290 eV) [9,29]. In addition, C–C, C–H, C–O, carboxyl, and carbonate groups in minor amounts could be observed for the BE. For the NMC811 electrodes (Fig. 5a), major differences in the spectra were also observed after adding PhEPi and VC to the BE. However, the observed bands differ severely from the features observed for the SiC electrode.

For the electrode from the cell cycled with BE + PhEPi compared to the cell cycled with BE, the band around 1160 cm^{-1} could be observed, which can be assigned to the P═O stretching vibrations, and several additional bands were observed around 1215, 1245, and 1280 cm^{-1}, which can be assigned to different semi-carbonates [23,46,48–50]. The more pronounced presence of the P═O bond is in line with the proposed mechanism for phospholanes on NMC [23]. From elemental XPS analysis, no change in carbon content for CEI in presence of PhEPi was observed compared to the BE, although an increase in the amount of oxygen can be seen. Low concentrations (~2–4%) of fluorophosphate

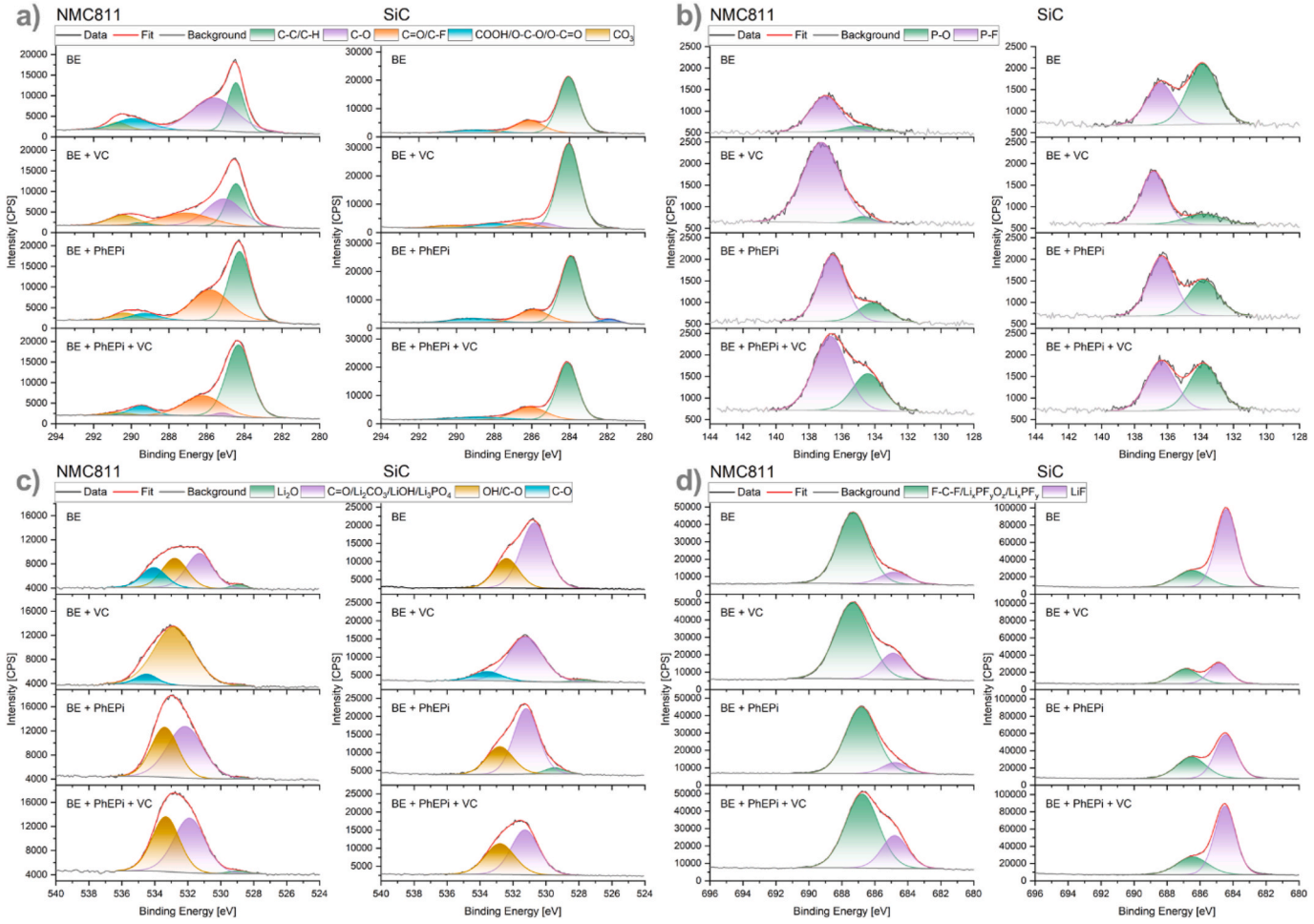

Fig. 7. XPS fitting results of the considered electrolyte formulations for (a) C 1s spectra, (b) P 2p spectra, (c) O 1s spectra, d) F 1s spectra as recorded for SiC and NMC811 after three formation cycles.

species, P–F bond (~137.0 eV), and P–O bond(~134.0 eV) were observed in P 2p spectra (Fig. 7b). In this figure, a significant increase in the P–O type bond for BE + PhEPi compared to BE was observed. Obtained XPS results concur with the finding of Raman analysis. O 1s region (Fig. 7c) comprised four distinct peaks assigned to the following bond types: C–O (~534.0 eV), C–O, carbonate type bonding and P–O species (~532–533 eV), and Li_2O (529 eV). For electrodes used with PhEPi, a higher C═O and P–O species concentration is observed in the formed CEI, which is in agreement with the other stated findings, while they have a lower concentration of C–O bond and carbonate species compared to the BE.

In Raman spectra, some changes were observed for the NMC electrode after adding VC to the BE + PhEPi. It also has to be noted that the intensity of the NMC lattice bands severely decreased compared to BE and BE + PhEPi. Besides, these bands assigned to the NMC material, again, bands around 1160 (P═O stretching) and 1308 cm^{-1} were observed [56], which can be ascribed to PhEPi. Moreover, a band around 960 cm^{-1} was observed, indicating the presence of LiF. This band was only observed for the BE + PhEPi + VC sample. The F 1s spectra for all the electrodes show peaks corresponding to LiF (~685 eV) and $Li_xPF_yO_z$/Li_xPF_y (~687 eV). Fig. 7d shows that using VC in the electrolyte formulations increases the amount of LiF formed on the NMC surface, which can also be seen in the highest amount for BE + PhEPi + VC. In addition, bands around 1215, 1245, and 1280 cm^{-1} in the Raman spectrum were detected, which can be assigned to the C–C and C–H stretching vibrations of olefinic Li-alkyl carboxylates [53].

Additionally, bands around 1400, 1465, and 1522 cm^{-1} were observed, indicating the increased presence of semi-carbonates [54,57,58]. The performed investigation also confirmed the presence of VC on the sample. Bands around 1572 and 1672 cm^{-1} were assigned to the CO_2 and C═C vibrations of pure VC [59]. However, Raman results show that amount of semi-carbonate species is increasing in the presence of VC. The elemental composition graph of the CEI formed in VC containing electrolytes shows a significant decrease in carbon content from 51% to 37% compared to the BE, and an increase in Li, F, and P concentration. This could indicate the decomposition of the VC molecules instead of polymerization on the surface of the electrode. We can correlate this observation to the decomposition peak in the cyclic voltammogram of BE + VC on NMC811 in Fig. 1d. This can also be an indication of pronounced decomposition and contribution of $LiPF_6$ to the CEI structure that can explain the observed lower initial discharge capacity for VC containing electrolyte in Fig. 2a. A combination of PhEPi + VC also showed a decrease in carbon content and an increase in the amount of Li, similar to VC alone. Furthermore, semi-carbonates in increased amounts were observed on the NMC electrode in the presence of VC containing electrolyte.

3.4.2. *Anode electrolyte interphase characteristics on SiC*

In Raman spectra, in addition to the vibration modes of the electrode bulk, many additional bands related to SEI were observed for the SiC electrode in BE (Fig. 5b). The bands around 888 and 1461 cm^{-1} correspond to the C═O and C–H stretching vibrations of the carbonate and the alkylic groups of different semi-carbonates (*e.g.*, DEDOHC, LEC, LMC), present as components of the SEI [54,55] while the band around

750 cm^{-1} can be allocated to Li_2CO_3 species. The bands around 1215, 1240, and 1287 cm^{-1} can be either assigned to C–C or C–H stretching vibrations of olefinic Li-alkyl carboxylates [53].

An additional band related to the SEI band, as a small shoulder next to the silicon band around 497 cm^{-1}, is assigned to Li_2O [2]. In general, it can be stated that presence of BE in the cell during galvanostatic cycling results in the formation of an SEI composed of known components (Li_2CO_3, Li_2O, and semi-carbonates) on the SiC electrode. The significant amount of C–C species and carbonyl group present in the C 1s region for BE (Fig. 7a) indicates that organic carbonate solvents decompose during galvanostatic cycling [60,61], as consistent with Raman results. Furthermore, O 1s spectra confirmed the presence of species like Li_2CO_3 and Li_2O in the formed SEI in the presence of BE (Fig. 7c). The interphase of SiC electrodes showed significant composition changes upon adding PhEPi and VC to the electrolyte formulation. For the cell galvanostatically cycled with BE + PhEPi, the presence of PhEPi molecules can be observed on the SiC surface by Raman spectroscopy. The corresponding band around 1025 cm^{-1} can be assigned to the P–*O*–C stretching vibration of PhEPi after comparison with the reference spectrum of the pure PhEPi (Fig. S4) [56]. This band was also observed for the electrode galvanostatically cycled in the cell containing BE + PhEPi + VC. However, additional bands were also observed, which could not be assigned to the additive. The band around 750 cm^{-1} can be ascribed to the formation of Li_2CO_3. Lithium carbonate and organic lithium carbonates are typically linear and cyclic carbonate reduction products [61]. The bands around 885 and 1455 cm^{-1} can be assigned to the C═O and C–H stretching vibrations of the carbonate and the alkylic groups of semi-carbonates [54,55]. Moreover, bands around 1223 and 1245 cm^{-1} were observed, ascribed to the C–C and C–H stretching vibrations of olefinic Li-alkyl carboxylates [53]. The presence of these bands and the prominent band around 1555 cm^{-1} indicate the increased presence of semi-carbonates on the surface of the electrode [56]. In addition, the presence of LiF might be indicated by the band around 690 cm^{-1} [62]. The SEI's elemental composition shows a significant increase in carbon concentration for PhEPi containing electrolyte (similar to Raman) and a slight decrease in Li and F concentration. On the SEI, for electrodes used with PhEPi, a lower C–O species concentration and a higher concentration of C═O bond and carbonate species were observed in C 1s spectra. Also, a significant increase in the P–O type bond was observed for BE + PhEPi and BE + PhEPi + VC compared to BE + VC. However, on SEI, a significant decrease in P–O species for all the electrolyte formulations can be seen compared to the BE. Additional bands, detected on the SiC surface for the BE + PhEPi + VC around 569, 646, 1107, and 1145 cm^{-1}, can be assigned to the polymerized VC [59]. The bands around 1107 and 1145 cm^{-1} correspond to the C–O stretching vibrations of poly(VC) [59]. VC polymerizes during galvanostatic cycling on the surface of the SiC electrode showing a clear fingerprint spectrum of poly(VC). Also, the absence of the band corresponding to C═C stretching vibrations of VC is another piece of evidence proving VC polymerization on the negative electrode, as observed in XPS elemental analysis and C 1s spectra (concentration of C–C and C–H type bonds increases in the presence of VC). In contrast to the SiC electrode, no indication of poly(VC) presence was observed on the NMC electrode. Instead, the band assigned to the C═C vibration of VC was detected. In contrast to VC, no bands indicating reaction or decomposition of PhEPi on the SiC electrode were observable. All bands assigned to PhEPi, match well with the recorded reference spectrum of the pure PhEPi. As seen in the cyclic voltammograms of BE + PhEPi (Fig. 1c), we could not assign any decomposition peak for PhEPi on SiC, which shows that PhEPi is not electrochemically active on SiC. We assume that PhEPi is strongly adsorbed on the anode surface, keeping the structure largely intact.

It can be concluded that decomposition products of the PhEPi on NMC811 and VC on both electrodes are found after three formation cycles. However, significant differences are observed in their influence on the SEI and CEI compositions.

4. Conclusions

The novel phospholane-based additive, PhEPi, at the optimum concentration in 1 M LiPF6 in EC:EMC 3:7 by vol. improves the cycling performance of NMC811||SiC cells in regard to the specific discharge capacity while fading, however, still remains an issue. The electrolyte formulation containing the optimum concentration of PhEPi and VC as co-additive, on the other hand, enhances the overall performance and prolongs the cycle life of NMC811||SiC cells in a synergistic fashion compared to the individual additives while outperforming FEC containing electrolyte. Obtained results prove that the novel electrolyte formulation is a promising alternative option to the FEC containing electrolytes in terms of electrochemical performance. The results of the systematic investigation of cell disassembly-reassembly strategy show that PhEPi plays a dominant role on the cathode and, in combination with VC, has a synergistic effect on both SEI and CEI. EIS analysis provides compelling evidence about the role of PhEPi and VC on the individual electrodes. PhEPi affects the internal cell resistance on the cathode, where it influences the CEI properties. *Post mortem* analysis comprising spectroscopic techniques of SHINERS and XPS supports the EIS results by observing PhEPi decomposition products on the NMC811 and the formation of an effective CEI. Furthermore, it was shown that decomposition of the VC molecules instead of polymerization on the NMC surface takes place in agreement with the CV measurements. In contrast, PhEPi adsorbs strongly on the SiC surface, which is assumed to bring a synergistic effect with VC on SiC, leading to improved overall NMC811||SiC cell performance.

Credit author statement

Bahareh A. Sadeghi: Methodology, Investigation, Formal analysis, Writing – original draft, Christian Wölke: Conceptualization, Investigation, Methodology, Writing – original draft, Writing-Reviewing and Editing, Felix Pfeiffer: Investigation, Masoud Baghernejad: Formal analysis, Martin Winter: Writing- Reviewing and Editing, Supervision, Isidora Cekic-Laskovic: Conceptualization, Methodology, Writing – original draft preparation, Supervision, Writing-Reviewing and Editing

Declaration of competing interest

The authors declare that they have no known competing financial interests or personal relationships that could have appeared to influence the work reported in this paper.

Data availability

Data will be made available on request.

Acknowledgment

The authors thank the European Research Council (ERC) for funding *via* the SeNSE project. This project has received funding from the European Union's Horizon 2020 research and innovation program under grant agreement No 875548.

Appendix A. Supplementary data

Supplementary data to this article can be found online at https://doi.org/10.1016/j.jpowsour.2022.232570.

References

[1] M. Greenwood, J.M. Wrogemann, R. Schmuch, H. Jang, M. Winter, J. Leker, The Battery Component Readiness Level (BC-RL) framework: a technology-specific development framework, J. Power Sources Adv. 14 (2022), 100089, https://doi.org/10.1016/j.powera.2022.100089.

[2] C. Naudin, J.L. Bruneel, M. Chami, B. Desbat, J. Grondin, J.C. Lassègues, L. Servant, Characterization of the lithium surface by infrared and Raman spectroscopies, J. Power Sources 124 (2003) 518–525, https://doi.org/10.1016/S0378-7753(03)00798-5.

[3] F. Tariq, V. Yufit, D.S. Eastwood, Y. Merla, M. Biton, B. Wu, Z. Chen, K. Freedman, G. Offer, E. Peled, P.D. Lee, D. Golodnitsky, N. Brandon, In-operando X-ray tomography study of lithiation induced delamination of Si based anodes for lithium-ion batteries, ECS Electrochem. Lett. 3 (2014) A76, https://doi.org/10.1149/2.0081407eel.

[4] D. Golodnitsky, K. Goldstein, K. Freedman, S. Menkin, E. Peled, Advanced multiphase silicon-based anodes for high-energy-density Li-ion and Li-air batteries, ECS Meet. Abstr. MA2014–04 (2014) 451, https://doi.org/10.1149/MA2014-04/2/451.

[5] Y. Arinicheva, M. Wolff, S. Lobe, C. Dellen, D. Fattakhova-Rohlfing, O. Guillon, D. Böhm, F. Zoller, R. Schmuch, J. Li, M. Winter, E. Adamczyk, V. Pralong, 10 - ceramics for electrochemical storage, in: O. Guillon (Ed.), Adv. Ceram. Energy Convers. Storage, Elsevier, 2020, pp. 549–709, https://doi.org/10.1016/B978-0-08-102726-4.00010-7.

[6] M. Winter, B. Barnett, K. Xu, Before Li ion batteries, Chem. Rev. 118 (2018) 11433–11456, https://doi.org/10.1021/acs.chemrev.8b00422.

[7] A. Gomez-Martin, F. Reissig, L. Frankenstein, M. Heidbüchel, M. Winter, T. Placke, R. Schmuch, Magnesium substitution in Ni-rich NMC layered cathodes for high-energy lithium ion batteries, Adv. Energy Mater. 12 (2022), 2103045, https://doi.org/10.1002/aenm.202103045.

[8] C. Wölke, B.A. Sadeghi, G.G. Eshetu, E. Figgemeier, M. Winter, I. Cekic-Laskovic, Interfacing Si-based electrodes: impact of liquid electrolyte and its components, Adv. Mater. Interfac. (2022), 2101898, https://doi.org/10.1002/admi.202101898.

[9] T. Placke, G.G. Eshetu, M. Winter, E. Figgemeier, Practical implementation of silicon-based negative electrodes in lithium-ion full-cells—challenges and solutions, Lithium-Ion Batter, Enabled Silicon Anodes (2021) 349–404, https://doi.org/10.1049/PBPO156E_ch11.

[10] Y. Jin, B. Zhu, Z. Lu, N. Liu, J. Zhu, Challenges and recent progress in the development of Si anodes for lithium-ion battery, Adv. Energy Mater. 7 (2017), 1700715, https://doi.org/10.1002/aenm.201700715.

[11] M.R. Wagner, P.R. Raimann, A. Trifonova, K.-C. Moeller, J.O. Besenhard, M. Winter, Electrolyte decomposition reactions on tin- and graphite-based anodes are different, Electrochem. Solid State Lett. 7 (2004) A201, https://doi.org/10.1149/1.1739312.

[12] M. Winter, W.K. Appel, B. Evers, T. Hodal, K.-C. Möller, I. Schneider, M. Wachtler, M.R. Wagner, G.H. Wrodnigg, J.O. Besenhard, Studies on the anode/electrolyte interfacein lithium ion batteries, Monatshefte Fuer ChemieChemical Mon 132 (2001) 473–486, https://doi.org/10.1007/s007060170110.

[13] M. Winter, The solid electrolyte interphase – the most important and the least understood solid electrolyte in rechargeable Li batteries, Z. Phys. Chem. 223 (2009) 1395–1406, https://doi.org/10.1524/zpch.2009.6086.

[14] J. Kasnatscheew, R. Wagner, M. Winter, I. Cekic-Laskovic, Interfaces and materials in lithium ion batteries: challenges for theoretical electrochemistry, in: M. Korth (Ed.), Model. Electrochem. Energy Storage at. Scale, Springer International Publishing, Cham, 2018, pp. 23–51, https://doi.org/10.1007/978-3-030-00593-1_2.

[15] E. Peled, The electrochemical behavior of alkali and alkaline earth metals in nonaqueous battery systems—the solid electrolyte interphase model, J. Electrochem. Soc. 126 (1979) 2047, https://doi.org/10.1149/1.2128859.

[16] D.R. Gallus, R. Wagner, S. Wiemers-Meyer, M. Winter, I. Cekic-Laskovic, New insights into the structure-property relationship of high-voltage electrolyte components for lithium-ion batteries using the pKa value, Electrochim. Acta 184 (2015) 410–416, https://doi.org/10.1016/j.electacta.2015.10.002.

[17] K. Kim, H. Ma, S. Park, N.-S. Choi, Electrolyte-additive-driven interfacial engineering for high-capacity electrodes in lithium-ion batteries: promise and challenges, ACS Energy Lett. 5 (2020) 1537–1553, https://doi.org/10.1021/acsenergylett.0c00468.

[18] F. Holtstiege, A. Wilken, M. Winter, T. Placke, Running out of lithium? A route to differentiate between capacity losses and active lithium losses in lithium-ion batteries, Phys. Chem. Chem. Phys. 19 (2017) 25905–25918, https://doi.org/10.1039/C7CP05405J.

[19] S.P. Kühn, K. Edström, M. Winter, I. Cekic-Laskovic, Face to face at the cathode electrolyte interphase: from interface features to interphase formation and dynamics, Adv. Mater. Interfac. 9 (2022), 2102078, https://doi.org/10.1002/admi.202102078.

[20] X. Fan, X. Ji, L. Chen, J. Chen, T. Deng, F. Han, J. Yue, N. Piao, R. Wang, X. Zhou, X. Xiao, L. Chen, C. Wang, All-temperature batteries enabled by fluorinated electrolytes with non-polar solvents, Nat. Energy 4 (2019) 882–890, https://doi.org/10.1038/s41560-019-0474-3.

[21] N. Piao, S. Liu, B. Zhang, X. Ji, X. Fan, L. Wang, P.-F. Wang, T. Jin, S.-C. Liou, H. Yang, J. Jiang, K. Xu, M.A. Schroeder, X. He, C. Wang, Lithium metal batteries enabled by synergetic additives in commercial carbonate electrolytes, ACS Energy Lett. 6 (2021) 1839–1848, https://doi.org/10.1021/acsenergylett.1c00365.

[22] H. Su, Z. Xie, J. Feng, Q. Wang, J. Zhou, Q. Fu, T. Meng, B. Huang, C. Meng, Y. Tong, Electrolyte additive strategy enhancing the electrochemical performance of a soft-packed LiCoO2//graphite full cell, Dalton Trans. 51 (2022) 8723–8732, https://doi.org/10.1039/D2DT01088G.

[23] G.G. Eshetu, E. Figgemeier, Confronting the challenges of next-generation silicon anode-based lithium-ion batteries: role of designer electrolyte additives and polymeric binders, ChemSusChem 12 (2019) 2515–2539, https://doi.org/10.1002/cssc.201900209.

[24] S. Klein, P. Harte, S. van Wickeren, K. Borzutzki, S. Röser, P. Bärmann, S. Nowak, M. Winter, T. Placke, J. Kasnatscheew, Re-evaluating common electrolyte additives for high-voltage lithium ion batteries, Cell Rep. Phys. Sci. 2 (2021), 100521, https://doi.org/10.1016/j.xcrp.2021.100521.

[25] S. Dühnen, J. Betz, M. Kolek, R. Schmuch, M. Winter, T. Placke, Toward green battery cells: perspective on materials and technologies, Small Methods 4 (2020), 2000039, https://doi.org/10.1002/smtd.202000039.

[26] T.R. Jow, Electrolytes for Lithium and Lithium-Ion Batteries, Springer, New York, 2014.

[27] D. Aurbach, K. Gamolsky, B. Markovsky, Y. Gofer, M. Schmidt, U. Heider, On the use of vinylene carbonate (VC) as an additive to electrolyte solutions for Li-ion batteries, Electrochim. Acta 47 (2002) 1423–1439, https://doi.org/10.1016/S0013-4686(01)00858-1.

[28] L.E. Ouatani, R. Dedryvère, C. Siret, P. Biensan, D. Gonbeau, Effect of vinylene carbonate additive in Li-ion batteries: comparison of LiCoO2 / C , LiFePO4 / C , and LiCoO2 / Li4Ti5O12 systems, J. Electrochem. Soc. 156 (2009) A468, https://doi.org/10.1149/1.3111891.

[29] M. Winter, R. Imhof, F. Joho, P. Novák, FTIR and DEMS investigations on the electroreduction of chloroethylene carbonate-based electrolyte solutions for lithium-ion cells, J. Power Sources 81–82 (1999) 818–823, https://doi.org/10.1016/S0378-7753(99)00116-0.

[30] T. Kennedy, M. Brandon, F. Laffir, K.M. Ryan, Understanding the influence of electrolyte additives on the electrochemical performance and morphology evolution of silicon nanowire based lithium-ion battery anodes, J. Power Sources 359 (2017) 601–610, https://doi.org/10.1016/j.jpowsour.2017.05.093.

[31] I.A. Profatilova, C. Stock, A. Schmitz, S. Passerini, M. Winter, Enhanced thermal stability of a lithiated nano-silicon electrode by fluoroethylene carbonate and vinylene carbonate, J. Power Sources 222 (2013) 140–149, https://doi.org/10.1016/j.jpowsour.2012.08.066.

[32] F. Aupperle, N. von Aspern, D. Berghus, F. Weber, G.G. Eshetu, M. Winter, E. Figgemeier, The role of electrolyte additives on the interfacial chemistry and thermal reactivity of Si-Anode-Based Li-ion battery, ACS Appl. Energy Mater. 2 (2019) 6513–6527, https://doi.org/10.1021/acsaem.9b01094.

[33] N. von Aspern, D. Diddens, T. Kobayashi, M. Börner, O. Stubbmann-Kazakova, V. Kozel, G.-V. Röschenthaler, J. Smiatek, M. Winter, I. Cekic-Laskovic, Fluorinated cyclic phosphorus(III)-Based electrolyte additives for high voltage application in lithium-ion batteries: impact of structure–reactivity relationships on CEI formation and cell performance, ACS Appl. Mater. Interfaces 11 (2019) 16605–16618, https://doi.org/10.1021/acsami.9b03359.

[34] X. Fan, C. Wang, High-voltage liquid electrolytes for Li batteries: progress and perspectives, Chem. Soc. Rev. 50 (2021) 10486–10566, https://doi.org/10.1039/D1CS00450F.

[35] C. Wölke, D. Diddens, B. Heidrich, M. Winter, I. Cekic-Laskovic, Understanding the effectiveness of phospholane electrolyte additives in lithium-ion batteries under high-voltage conditions, Chemelectrochem 8 (2021) 972–982, https://doi.org/10.1002/celc.202100107.

[36] R. Nölle, K. Beltrop, F. Holtstiege, J. Kasnatscheew, T. Placke, M. Winter, A reality check and tutorial on electrochemical characterization of battery cell materials: how to choose the appropriate cell setup, Mater. Today 32 (2020) 131–146, https://doi.org/10.1016/j.mattod.2019.07.002.

[37] R. Petibon, C.P. Aiken, N.N. Sinha, J.C. Burns, H. Ye, C.M. VanElzen, G. Jain, S. Trussler, J.R. Dahn, Study of electrolyte additives using electrochemical impedance spectroscopy on symmetric cells, J. Electrochem. Soc. 160 (2013), https://doi.org/10.1149/2.005302jes. A117–A124.

[38] J. Becking, A. Gröbmeyer, M. Kolek, U. Rodehorst, S. Schulze, M. Winter, P. Bieker, M.C. Stan, Lithium-metal foil surface modification: an effective method to improve the cycling performance of lithium-metal batteries, Adv. Mater. Interfac. 4 (2017), 1700166, https://doi.org/10.1002/admi.201700166.

[39] F. Ding, W. Xu, X. Chen, J. Zhang, M.H. Engelhard, Y. Zhang, B.R. Johnson, J. V. Crum, T.A. Blake, X. Liu, J.-G. Zhang, Effects of carbonate solvents and lithium salts on morphology and coulombic efficiency of lithium electrode, J. Electrochem. Soc. 160 (2013) A1894, https://doi.org/10.1149/2.100310jes.

[40] J.F. Li, X.D. Tian, S.B. Li, J.R. Anema, Z.L. Yang, Y. Ding, Y.F. Wu, Y.M. Zeng, Q. Z. Chen, B. Ren, Z.L. Wang, Z.Q. Tian, Surface analysis using shell-isolated nanoparticle-enhanced Raman spectroscopy, Nat. Protoc. 8 (2013) 52–65, https://doi.org/10.1038/nprot.2012.141.

[41] T. Wang, L. Rao, X. Jiao, J. Choi, J. Yap, J.-H. Kim, Impact of triethyl borate on the performance of 5 V spinel/graphite lithium-ion batteries, ACS Appl. Energy Mater. 5 (2022) 7346–7355, https://doi.org/10.1021/acsaem.2c00861.

[42] Y. Kobayashi, T. Kobayashi, K. Shono, Y. Ohno, Y. Mita, H. Miyashiro, Decrease in capacity in Mn-Based/Graphite commercial lithium-ion batteries: I. Imbalance proof of electrode operation capacities by cell disassembly, J. Electrochem. Soc. 160 (2013) A1181, https://doi.org/10.1149/2.071308jes.

[43] L. Gao, J. Chen, Q. Chen, X. Kong, The chemical evolution of solid electrolyte interface in sodium metal batteries, Sci. Adv. 8 (2022), eabm4606, https://doi.org/10.1126/sciadv.abm4606.

[44] L. Somerville, J. Bareño, P. Jennings, A. McGordon, C. Lyness, I. Bloom, The effect of pre-analysis washing on the surface film of graphite electrodes, Electrochim. Acta 206 (2016) 70–76, https://doi.org/10.1016/j.electacta.2016.04.133.

[45] B. Stiaszny, J.C. Ziegler, E.E. Krauß, J.P. Schmidt, E. Ivers-Tiffée, Electrochemical characterization and post-mortem analysis of aged LiMn2O4–Li(Ni0.5Mn0.3Co0.2)O2/graphite lithium ion batteries. Part I: cycle aging, J. Power Sources 251 (2014) 439–450, https://doi.org/10.1016/j.jpowsour.2013.11.080.

[46] T. Waldmann, A. Iturrondobeitia, M. Kasper, N. Ghanbari, F. Aguesse, E. Bekaert, L. Daniel, S. Genies, I.J. Gordon, M.W. Löble, E. De Vito, M. Wohlfahrt-Mehrens, Review—post-mortem analysis of aged lithium-ion batteries: disassembly

methodology and physico-chemical analysis techniques, J. Electrochem. Soc. 163 (2016) A2149, https://doi.org/10.1149/2.1211609jes. –A2164.
[47] A.U. Schmid, M. Kurka, K.P. Birke, Reproducibility of Li-ion cell reassembling processes and their influence on coin cell aging, J. Energy Storage 24 (2019), 100732, https://doi.org/10.1016/j.est.2019.04.006.
[48] N. Williard, B. Sood, M. Osterman, M. Pecht, Disassembly methodology for conducting failure analysis on lithium–ion batteries, J. Mater. Sci. Mater. Electron. 22 (2011) 1616, https://doi.org/10.1007/s10854-011-0452-4.
[49] A.L. Michan, S. Bharathy, Parimalam, M. Leskes, R.N. Kerber, T. Yoon, C.P. Grey, B.L. Lucht, Fluoroethylene carbonate and vinylene carbonate reduction: understanding lithium-ion battery electrolyte additives and solid electrolyte interphase formation, Chem. Mater. 28 (2016) 8149–8159, https://doi.org/10.1021/acs.chemmater.6b02282.
[50] Y. Jin, N.-J.H. Kneusels, L.E. Marbella, E. Castillo-Martínez, P.C.M.M. Magusin, R. S. Weatherup, E. Jónsson, T. Liu, S. Paul, C.P. Grey, Understanding fluoroethylene carbonate and vinylene carbonate based electrolytes for Si anodes in lithium ion batteries with NMR spectroscopy, J. Am. Chem. Soc. 140 (2018) 9854–9867, https://doi.org/10.1021/jacs.8b03408.
[51] A. Shodiev, E.N. Primo, M. Chouchane, T. Lombardo, A.C. Ngandjong, A. Rucci, A. A. Franco, 4D-resolved physical model for Electrochemical Impedance Spectroscopy of Li(Ni1-x-yMnxCoy)O2-based cathodes in symmetric cells: consequences in tortuosity calculations, J. Power Sources 454 (2020), 227871, https://doi.org/10.1016/j.jpowsour.2020.227871.
[52] M. Steinhauer, S. Risse, N. Wagner, K.A. Friedrich, Investigation of the solid electrolyte interphase formation at graphite anodes in lithium-ion batteries with electrochemical impedance spectroscopy, Electrochim. Acta 228 (2017) 652–658, https://doi.org/10.1016/j.electacta.2017.01.128.
[53] M.J. Piernas-Muñoz, A. Tornheim, S. Trask, Z. Zhang, I. Bloom, Surface-enhanced Raman spectroscopy (SERS): a powerful technique to study the SEI layer in batteries, Chem. Commun. 57 (2021) 2253–2256, https://doi.org/10.1039/D0CC08001B.
[54] A. Gajan, C. Lecourt, B.E. Torres Bautista, L. Fillaud, J. Demeaux, I.T. Lucas, Solid electrolyte interphase instability in operating lithium-ion batteries unraveled by enhanced-Raman spectroscopy, ACS Energy Lett. 6 (2021) 1757–1763, https://doi.org/10.1021/acsenergylett.1c00436.
[55] G. Li, H. Li, Y. Mo, L. Chen, X. Huang, Further identification to the SEI film on Ag electrode in lithium batteries by surface enhanced Raman scattering (SERS), J. Power Sources 104 (2002) 190–194, https://doi.org/10.1016/S0378-7753(01)00908-9.
[56] G. Socrates, in: Infrared and Raman Characteristic Group Frequencies: Tables and Charts vol. 3, Wiley, Chichester, 2010. Repr. As Paperback.
[57] S.-Y. Ha, J.-G. Han, Y.-M. Song, M.-J. Chun, S.-I. Han, W.-C. Shin, N.-S. Choi, Using a lithium bis(oxalato) borate additive to improve electrochemical performance of high-voltage spinel LiNi0.5Mn1.5O4 cathodes at 60°C, Electrochim. Acta 104 (2013) 170–177, https://doi.org/10.1016/j.electacta.2013.04.082.
[58] M. Tammer, G. Sokrates, Infrared and Raman characteristic group frequencies: tables and charts, Colloid Polym. Sci. 283 (2004), https://doi.org/10.1007/s00396-004-1164-6, 235–235.
[59] H. Ota, Y. Sakata, A. Inoue, S. Yamaguchi, Analysis of vinylene carbonate derived SEI layers on graphite anode, J. Electrochem. Soc. 151 (2004) A1659, https://doi.org/10.1149/1.1785795.
[60] V. Shutthanandan, M. Nandasiri, J. Zheng, M.H. Engelhard, W. Xu, S. Thevuthasan, V. Murugesan, Applications of XPS in the characterization of Battery materials, J. Electron. Spectrosc. Relat. Phenom. 231 (2019) 2–10, https://doi.org/10.1016/j.elspec.2018.05.005.
[61] M.N. Vila, E.M. Bernardez, W. Li, C.A. Stackhouse, C.J. Kern, A.R. Head, X. Tong, S. Yan, L. Wang, D.C. Bock, K.J. Takeuchi, L.M. Housel, A.C. Marschilok, E. S. Takeuchi, Interfacial reactivity of silicon electrodes: impact of electrolyte solvent and presence of conductive carbon, ACS Appl. Mater. Interfaces 14 (2022) 20404–20417, https://doi.org/10.1021/acsami.1c22044.
[62] S. Tang, Y. Gu, J. Yi, Z. Zeng, S.-Y. Ding, J.-W. Yan, D.-Y. Wu, B. Ren, Z.-Q. Tian, B.-W. Mao, An electrochemical surface-enhanced Raman spectroscopic study on nanorod-structured lithium prepared by electrodeposition, J. Raman Spectrosc. 47 (2016) 1017–1023, https://doi.org/10.1002/jrs.4970.